Slow Dynamic Processes in Lead Halide Perovskite Solar Cells. Characteristic Times and Hysteresis

ARTICLE *in* JOURNAL OF PHYSICAL CHEMISTRY LETTERS · JUNE 2014

Impact Factor: 7.46 · DOI: 10.1021/jz5011187

THE JOURNAL OF PHYSICAL CHEMISTRY Letters

Letter

pubs.acs.org/JPCL

Slow Dynamic Processes in Lead Halide Perovskite Solar Cells. Characteristic Times and Hysteresis

Rafael S. Sanchez,[†] Victoria Gonzalez-Pedro,[†] Jin-Wook Lee,[‡] Nam-Gyu Park,*[,‡] Yong Soo Kang,[§] Ivan Mora-Sero,*[,†] and Juan Bisquert*[,†,∥]

[†]Photovoltaics and Optoelectronic Devices Group, Departament de Física, Universitat Jaume I, 12071 Castelló, Spain

[‡]School of Chemical Engineering and Department of Energy Science, Sungkyunkwan University, Suwon 440-746, South Korea

[§]Center for Next Generation Dye-Sensitized Solar Cells, Department of Energy Engineering, Hanyang University, Seoul 133-791, South Korea

[∥]Department of Chemistry, Faculty of Science, King Abdulaziz University, Jeddah, Saudi Arabia

Supporting Information

ABSTRACT: Characteristic times of perovskite solar cells (PSCs) have been measured by different techniques: transient photovoltage decay, transient photoluminescence, and impedance spectroscopy. A slow dynamic process is detected that shows characteristic times in the seconds to milliseconds scale, with good quantitative agreement between transient photovoltage decay and impedance spectroscopy. Here, we show that this characteristic time is related with a novel slow dynamic process caused by the peculiar structural properties of lead halide perovskites and depending on perovskite crystal size and organic cation nature. This new process may lie at the basis of the current−voltage hysteresis reported for PSCs and could have important implications in PSC performance because it may give rise to distinct dynamical behavior with respect to other classes of photovoltaic devices. Furthermore, we show that low-frequency characteristic time, commonly associated with electronic carrier lifetime in other photovoltaic devices, cannot be attributed to a recombination process in the case of PSCs.

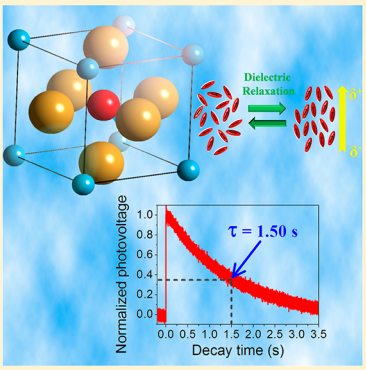

SECTION: Energy Conversion and Storage; Energy and Charge Transport

Hybrid organic−inorganic lead halide perovskite (PS)[1,2] derivatives are becoming one of the most promising materials for sunlight energy conversion, mainly due to the high overall cell efficiency, with certified values as high as 17.9%, and the rapid rate of improvement that they have experienced in the last years.[3−8] There has been a significant amount of work on the topic recently, but many points of the different physical processes acting on this kind of cells are not completely understood. Therefore, devoting a great effort toward the elucidation of the working principles of perovskite solar cells (PSCs) is needed. A great variety of recent works can be found in the literature aimed to improving the power conversion efficiency, η, of the devices by modifying the PS deposition methodologies, for example, single[4,6,9] or sequential step procedures,[4,3] as well as by varying the nature of the PS precursors employed, that is, halides (Cl^-, Br^-, I^-)[10−12] or organic (methylammonium, formamidinium)[11,13,14] or inorganic cations (Pb^{2+}, Sn^{2+}).[15−17] Unfortunately, it is yet unknown what is the exact influence of the film growth methodologies and/or nature of the precursors over the mechanisms ruling the overall performance of the devices. In addition, there are several pieces of evidence that point to new features and physical processes occurring in PSCs. For instance, recent studies have identified an anomalous hysteresis in PS solar cells, and although several hypotheses have been proposed, its origin remains still unclear.[18] In addition, the observed distinct characteristic arc in impedance spectroscopy (IS) at low frequencies[19] is another fact that requires explanation.

In this work, we report the dynamics characteristics of the PSCs in the slow time scale pertinent to photovoltaic operation. We combine time domain and frequency domain measurements, and we propose that photovoltage decay times in PSCs are governed by a new slow reorganization process that is intrinsic to the structural features of the material. We discuss the correlation of photovoltage decay times with the cell performance, and we show that slow time domain characteristic times do not straightforwardly correspond to a recombination as they are influenced by the intrinsic reorganization process of the PS structure.

In order to test PSC dynamic processes, we compare two different methodologies of PS deposition, a single ($CH_3NH_3PbI_{3-x}Cl_x$) and a sequential step ($CH_3NH_3PbI_3$) procedure, and the use of two types of organic cations, methylammonium (MA) and formamidinium (FA), with a clearly differentiated dipole moment, 2.28 and 0.21 D,

Received: June 3, 2014
Accepted: June 18, 2014
Published: June 18, 2014

   dx.doi.org/10.1021/jz5011187 | J. Phys. Chem. Lett. 2014, 5, 2357−2363

respectively.[20] The PS films were deposited on nanostructured TiO_2 substrates (NS-TiO_2); see the Supporting Information for further details. From now, they will be referred as *Sing*-MA/I-Cl for single step growth of $CH_3NH_3PbI_{3-x}Cl_x$, in which all of the precursors are mixed and deposited using a single spin coating step, *Seq*-MA/I for sequential deposition of $CH_3NH_3PbI_3$, and *Seq*-FA/I for sequential formation of $CH(NH_2)_2PbI_3$. In sequential deposition, PbI_2 is deposited first by spin coating, while in a second step, the PbI_2 sample is dipped in a solution of the organic cation for the final formation of the PS.[3]

After the preparation of the above-mentioned devices, the current−voltage (J/V) curves of the three types of cells were registered, Figure 1, and the corresponding cell performance

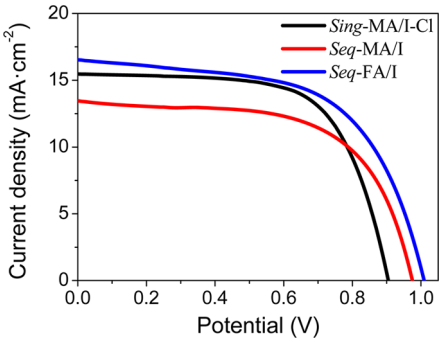

Figure 1. J/V curves of the three types of PS-based devices. Measurements were carried out under 1 sun illumination (AM1.5G, 100 mW cm^{-2}) and sweeping voltages in the scan− direction with a scan rate of s = 50 mV/s.

Table 1. Cell Parameters of PSCs Extracted from J/V Curves Depicted in Figure 1[a]

sample	J_{sc} (mA·cm^{-2})	V_{oc} (V)	FF (%)	η (%)
Sing-MA/I-Cl	15.5	0.904	65.5	9.2
Seq-MA/I	13.5	0.974	61.4	8.0
Seq-FA/I	16.5	1.009	59.0	10.9

[a]Variables: short-circuit photocurrent, J_{sc}; open circuit voltage, V_{oc}; fill factor, FF; and photoconversion efficiency, η.

parameters are shown in Table 1. J/V curves and parameters in Figure 1 and Table 1 have been obtained by scanning voltages sweeping from high voltages to zero applied voltage. We will denote hereafter this J/V scan as scan−, as opposed to scan+, where the voltage is swept from zero voltage to high voltage. As can be observed, in all cases, the efficiencies of the devices are comparable with averaged values reported in the literature. Consequently, reliable and comparable conclusions can be extracted from the analysis of these samples. It is worth pointing out that devices prepared by the sequential methodology in this work yielded systematically higher open-circuit (V_{oc}) values, thus revealing a preliminary effect of the PS growth conditions on the performance of the solar cells. The light absorption of different samples is plotted in Figure S1 (Supporting Information), where it can be appreciated that there is a red shift of the PS band gap when FA is used instead of MA, as has been previously reported.[11,14]

Although comparable efficiencies and cell parameters were obtained for each device, a differentiated behavior was observed after a deeper electrical and electro-optical characterization. A broadly used approach to unravelling the charge dynamics of solar cell devices is the small perturbation transient photovoltage decay (TPD). Experiments were carried out by using a white LED to vary the back illumination level and a nanosecond-pulsed Nd/YAG laser (λ_{exc}= 650 nm) to promote the voltage perturbation (≈20 mV). It is widely assumed that the transient photovoltage is a suitable technique for determining the electron recombination lifetime (τ_{rec}) in dye-sensitized solar cells (DSCs).[21,22] Recent reports on solid-state solar cells based on lead halide PS adopt the same reasoning for studying the electron recombination kinetics. For instance, Bi et al.[23] and Zhao et al.,[24] reported the photovoltage decay times by fitting the transient signals to a monoexponential function. On the contrary, Listorti and co-workers reported on a double decay time contribution,[25] as well as Park and co-workers.[26] In this case, slow and fast time components were resolved, which were ascribed to an electron recombination pathway in the PS film and an additional mechanism for the electrons injected into the TiO_2. Note that in our previous work, we have determined the diffusion length in PSCs from transport and recombination resistance and not from characteristic times determined from impedance.[27]

Despite the precedents mentioned above, our transient photovoltage results reveal a very different behavior depending on the PS deposition procedures. Figure 2a shows the TPD times at different back illumination intensities obtained for those samples analyzed in the present work. The signals were

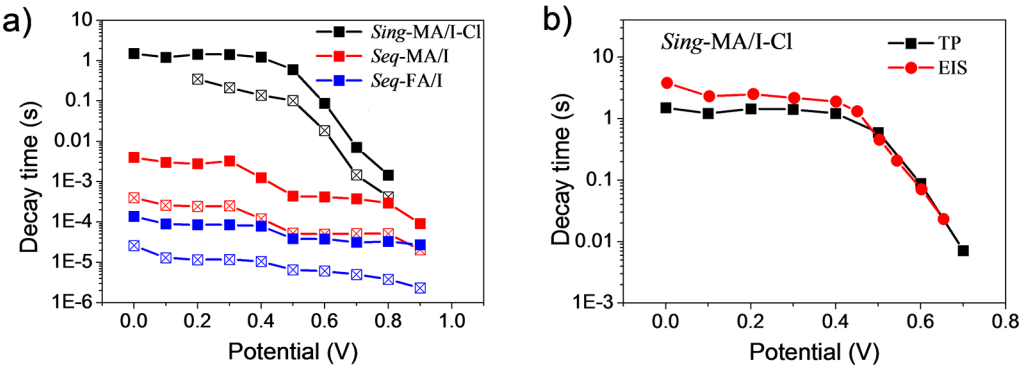

Figure 2. (a) TPD times at different back illumination intensities of the PS-based devices with *Sing*-MA/I-Cl, *Seq*-MA/I, and *Seq*-FA/I from the fitting to a biexponential function. (Solid square) τ_1; (crossed square) τ_2. (b) Comparison between the TPD time τ_1 with the characteristic time obtained at low frequency from IS. Both measurements were performed at different open-circuit conditions by changing the light intensity.

dx.doi.org/10.1021/jz5011187 | *J. Phys. Chem. Lett.* 2014, 5, 2357−2363

fitted accurately to biexponential functions, however, while the *Sing*-MA/I-Cl sample showed TPD times, τ_1 and τ_2, in the seconds to milliseconds scale, the *Seq*-MA/I and *Seq*-FA/I decays were in the milliseconds to microseconds range. The results plotted in Figure 2a indicate that the retrieved characteristic times cannot be associated with recombination lifetimes and point to an additional significantly slow process contributing to the photovoltage decay. Several facts support this conclusion. Extremely large characteristic times are obtained for *Sing*-MA/I-Cl, even longer than that in liquid electrolyte DSCs, when a recombination more rapid than that on solid devices should be expected.[21,25] In addition, the *Sing*-MA/I-Cl samples that present the longest characteristic times also present the lowest V_{oc}, as discussed further below.

In Figure 2b is depicted a comparison between the TPD time τ_1 with the characteristic time obtained at low frequency from IS. There is good agreement between the characteristic times obtained by both characterization techniques. In the case of DSCs, is well known that both techniques provide the same values, being in that case the electronic carrier recombination lifetime.[22] In the following, we argue that in the case of PSCs, the characteristic time obtained by both techniques is related to a slow dynamic process.

The standard interpretation of photovoltage decays and the recombination lifetime have been established in terms of the decay of the Fermi level in an otherwise homogeneous environment, as illustrated in Figure 3a.[28] In this model, the

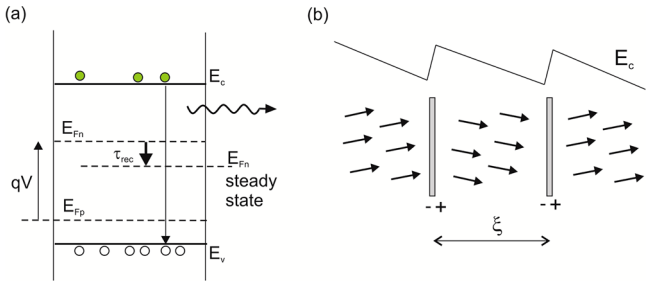

Figure 3. (a) Concept of the recombination lifetime, showing the conduction band edge E_c, the Fermi level of electrons E_{Fn}, the dark equilibrium Fermi level E_{F0}, and the recombination lifetime τ_{rec}. (b) Scheme showing domains of net polarization with a correlation length ξ. Thus, the charge is accumulated at the domain wall (interfaces), and the band is tilted inside of the domain. At the domain wall, opposite charges exist at the two sides; therefore, a local dipole is formed.

transition of the Fermi level E_{Fn} toward the steady-state value imposed by background illumination occurs with an exponential function governed by the lifetime τ_{rec}. The lifetime is therefore an exclusive feature of the recombination of minority carriers. The same conclusion is obtained by measuring IS, where independently the chemical capacitance C_μ and recombination resistance R_{rec} can be determined and they provide the recombination lifetime as[22]

$$\tau_{rec} = R_{rec} C_\mu \quad (1)$$

It has been established that τ_{rec} shows additional dynamic processes besides the recombination event. In particular, electron traps increase the chemical capacitance and elongate the values of τ_{rec}. This is the reason why in a DSC, the lifetime continuously decreases at increasing open-circuit voltage. These features have been amply explained by modeling and measurement.[29−31] However, it is generally expected for cells that provide a similar photocurrent that the one with the longest recombination lifetime will produce the largest V_{oc} as a consequence of decreased recombination rate. This general axiom of DSCs is broken in the PSCs probed in this work as the FAI cells provide the largest voltage while they show the shortest decay time. This observation requires a reinterpretation of the slowest characteristic time observed in the PSCs because a shorter time appears to be beneficial for the photovoltaic performance in this case.

Frequency domain IS measurements of PSCs have been already developed in our group.[19] One important observation is that this type of cells often presents an additional arc at low frequency, as shown in Figure 4a, that provokes a major impact

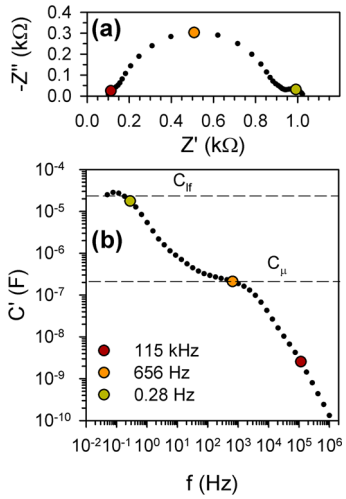

Figure 4. IS (a) complex impedance plot (imaginary part of the impedance, Z'', versus the real part, Z') and (b) Bode plot of the real part of the capacitance, C', obtained for a *Sing*-MA/I-Cl sample under dark conditions at 0.9 V applied DC bias. Three frequencies are highlighted to distinguish low-, intermediate-, and high-frequency regions.

in the dynamics of electronic processes. In the complex impedance plot, three arc features at low-, intermediate-, and high-frequency (lf, if, and hf, respectively) are clearly indentified. The hf arc is associated with selective contacts,[27,32,33] and the arc at if is associated with the chemical capacitance; see Figure 4b.[19] However, the origin of the third arc at lf was not previously described.

Focusing on the lf arc process, in DSCs, it is very common to observe an additional third arc at low frequency when the redox species are immersed in a viscous medium as an ionic liquid.[34] However, it has been established that series processes in solid-state cells mainly occur in the high-frequency range,[35] and a similar conclusion has been reached in the analysis of PSCs.[36] Therefore, the lowest-frequency process observed in PSC cells cannot be viewed as an obvious series process. In addition, the slow dynamic process is accompanied by a new physical feature that is unprecedented in any of the known solar cell types. There is a major increase of the capacitance at low frequency, C_{lf}, that goes well beyond the value of the chemical capacitance, as shown in Figure 4b. Such a feature could be explained in terms of the ferroic properties of the PS structure. Therefore, the low-frequency arc appears to be related to the dielectric relaxation process shown in Figure 3b. Polarization is created by aligning dipoles or dipolar domains to the external electrical field. The origin of the dipolar units is the dipole moment of

dx.doi.org/10.1021/jz5011187 | J. Phys. Chem. Lett. 2014, 5, 2357−2363

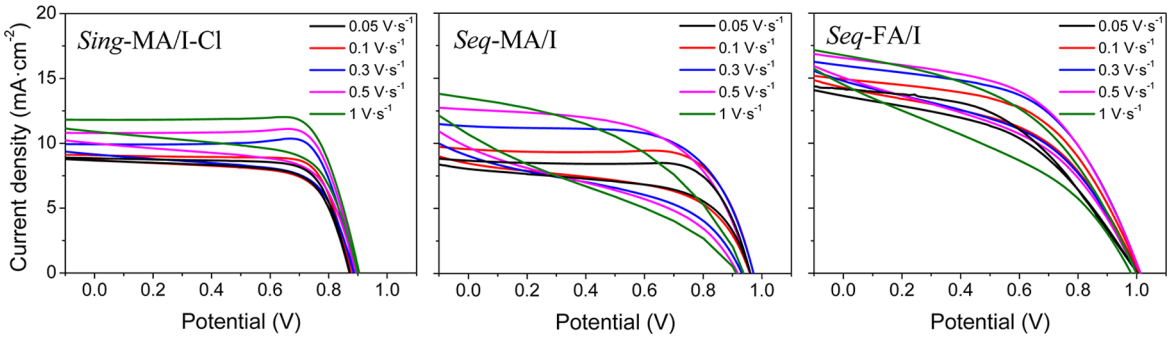

Figure 5. Cyclic voltammetries at different scan rates of the three different sets of samples under the solar simulator conditions.

the organic cation as well as the easy distortion of the PS framework. The rearrangement of the overall orientation in response to any external perturbation occurs in a slow time dynamics. If the correlation length ξ of the polarized domains is much smaller than the sample size or even than grain size (as expected for weak dipole−dipole interactions), then the effects of charge separation will be local. A number of interesting phenomena appear because the polarized domains may affect the electronic carrier dynamics by diverting them to domain walls where polarization mismatch may create abrupt band bending features, Figure 3b. The specific nature of the slow relaxation will probably require extensive investigation, but here, we wish to point out that the behavior appears to be dominated by structural relaxation, while electronic carrier dynamics is strongly influenced by this process.

It is worth commenting that the IS patterns obtained for PSCs may present different features depending on the sample, the applied bias, or the illumination conditions, and in many cases, some of the above processes are merged in the measured spectra. In addition, at high applied DC bias, a new feature presenting negative capacitance is observed, preventing the observation of the lf arc; see Figure S2, Supporting Information. Negative capacitance has been previously observed in other photovoltaic devices, and its origin is still under debate.[37]

In Figure 2b, we show that the time constant obtained by both methods, the photovoltage decay and the low-frequency arc of the IS response, is the same to a very good approximation for *Sing*-MA/I-Cl, which corroborates the effect of the dielectric polarization on the photovoltage response. These results also suggest that the magnitude of the dielectric polarization is sensitive to the PS crystal growth procedure. Although this work is not focused on unravelling the crystallographic properties of PS, we hypothesize that this phenomenon could be ascribed to the formation of different crystal morphologies depending on the deposition methodology. In principle, a fast recombination kinetics should induce more efficient losses in the charge collection, thus contributing to a detrimental effect on the efficiency. As remarked before, our results show that devices with very differentiated photovoltage decay times afford comparable efficiencies; in fact, the sample *Seq*-FA/I showed the fastest decay times but contrarily yielded the highest V_{oc}. Consequently, TPD measurements do not unambiguously yield the electron lifetime in solid-state PS devices.

The time constant obtained by TPD or IS (closed- to open-circuit conditions) should be equivalent because both methods measure the small perturbation of the Fermi level at the contact. This is confirmed by the expected agreement of the two measurements in Figure 2b. The problem that we face here is the interpretation of the measured response time, which has the structure $\tau = RC$. We have shown above that the capacitance $C(\omega)$ has a complex frequency-dependent structure, so that it may be formed by a combination of chemical and polarization capacitances. Thus, the response time cannot be generally interpreted as a recombination lifetime (eq 1) because other types of relaxation behavior influence the decay of the photovoltage. In order to separate the different effects, it is necessary to develop a full impedance model that takes into account the different phenomena and provides the relevant parameters. This work is out of the scope of this Letter and is currently in progress.

From a general point of view, the low-frequency relaxation phenomenon seems to play a significant role on a wide number of photoelectrochemical processes that take place in the solar cells. One prominent example of irregular behavior of slow dynamics in the PSCs cells is the hysteresis of the current−voltage curve, which is a significant effect in that the solar cell efficiency depends dramatically on the sense of measurement in the voltage axis and on the velocity of the voltage scan. Many groups worldwide have noted the existence, and it has also been reported in papers.[18,32] However, no conclusive outcomes about the origin of this capacitive effect were provided. Instead, it was suggested that this phenomenon must obey an intrinsic property of the PSCs because PS was the common denominator for samples experiencing hysteresis.[18] In addition, Snaith and co-workers observed that the magnitude of this effect increased while the scan rate was reduced.[18] On the contrary, Dualeh et al. reported an opposite dependence of the hysteresis with the scan rate.[32]

Here, we report on the presence of the same hysteresis effect in the J/V curve, as can be observed in Figure 5. To quantify the hysteresis effect, we have defined an adimensional hysteric index (HI) as

$$\mathrm{HI} = \frac{J_{\mathrm{scan-}}(V_{oc}/2) - J_{\mathrm{scan+}}(V_{oc}/2)}{J_{\mathrm{scan-}}(V_{oc}/2)} \qquad (2)$$

where $J_{\mathrm{scan-}}(V_{oc}/2)$ is the photocurrent at $V_{oc}/2$ bias for the scan−, while $J_{\mathrm{scan+}}(V_{oc}/2)$ is the photocurrent for the scan+. A HI of 0 corresponds to a cell without significant hysteresis, while a HI of 1 corresponds to a system in which the hysteresis is as high as the photocurrent. HIs obtained for the analyzed samples at different scan rates, *s*, are listed in Table 2.

In our case, a general trend was observed concerning the influence of the scan rate on the hysteresis; see Table 2. Specifically, our results show that the hysteresis is enhanced at high sweep rates, and it is also enhanced under illumination; see Figure S3, Supporting Information. Furthermore, the magnitude of the hysteresis event is clearly sensitive to the conditions

dx.doi.org/10.1021/jz5011187 | J. Phys. Chem. Lett. 2014, 5, 2357−2363

Table 2. Hysteresis Factor Extracted from Data in Figure 5 Using the Definition Provided in Equation 2 for Different Scan Rates, *s*

s ($V \cdot s^{-1}$)	*Sing*-MA/I-Cl	*Seq*-FA/I	*Seq*-MA/I
0.05	0.04	0.08	0.16
0.1	0.08	0.11	0.22
0.3	0.16	0.18	0.39
0.5	0.16	0.22	0.44
1	0.16	0.30	0.44

and/or precursors utilized for the PS growth. On one hand, the sample prepared with a single step and using a Cl precursor, *Sing*-MA/I-Cl, presents the lowest HI. On the other hand, comparing samples prepared by the same experimental procedure, using sequential deposition, *Seq*-FA/I showed lower hysteresis compared to that of devices with the MA precursor.

In general, in a solar cell, we may distinguish the capacitive and noncapacitive current. The latter is the only one pertinent to steady-state performance because solar cells operate at steady state. Extraction of photogenerated charge and recombination are normally noncapacitive and produce the diode curve response characteristic of all solar cells. Noncapacitive currents depend on the given value of the voltage and hence have the same value independent of the variation rate of the voltage. On the other hand, for a capacitive current, the situation is very different. According to the formula known from cyclic voltammetry measurements, the capacitive current depends on the voltage sweep direction and rate as[38]

$$J_{\text{capacitive}} = \frac{dQ}{dt} = C\frac{\Delta V}{\Delta t} = Cs \tag{3}$$

where Q is charge, C is capacitance, and s is the scan rate. Note that the capacitive current is reversed when the sign of the voltage step ΔV is exchanged in a scan+ and scan− sweeps. Furthermore, when the time step Δt, used in the measurement of the J/V curve, is shorter, the asymmetrical capacitive current increases. These considerations explain well the observations reported in Table 2, with increasing hysteresis at larger scan rates. We note that this type of feature has been widely recognized in liquid electrolyte DSCs, which share the feature of a large (chemical) capacitance.[39] However, in PSC, the large low-frequency capacitance associated with dielectric relaxation makes the hysteretic feature even larger. It is important to point out that this is a transient effect that according to eq 3 can be practically eliminated by performing a rather slow measurement. The truly significant efficiency for solar energy conversion is the steady-state efficiency. Adequate measurement protocols that take into account the large intrinsic capacitance may be developed. Of course, the larger the capacitance, the more time-consuming will be the procedure to obtain the J/V curve with high accuracy.

These facts point to a relationship between slow dynamic processes previously discussed in this work and the hysteresis effect. Slow dynamics is connected, as mentioned before, to a large capacitance at low frequency that is furthermore enhanced by illumination. Hysteresis then depends on both growth conditions and the type of PS, indicating an intrinsic effect governed by the grain size and organic cation nature. Previous works in the literature indicate that the organic cation, that is, MA or FA, seems to play a significant role in the cell performance.[11] Because the FA cation has a significant lower dipole moment,[20] this would be in agreement with the lower hysteresis observed for *Seq*-FA/I. In addition, PS growth with Cl precursors produces large crystal grains[40] affecting also the polarization effects; see Figure 2b. Therefore, our results suggest that the dielectric polarization is the main reason for the J/V hysteresis.

It is tempting to attribute a direct role of the electrical field in the changing behavior of the J/V curve depending on the scan rate. It must be noted however that the PSCs show a rather long diffusion length; therefore, the role of electrical field in charge collection may not necessarily be predominant. In addition, it has been recently shown that a large photovoltage in PSC is determined by the separation of Fermi levels in the absorber, not by the contact materials.[19,41] Therefore, the significance of a built-in field in charge separation is not established yet. As stated above, the main factor controlling the transient J/V hysteresis is the large capacitance induced by dielectric relaxation, although additional contributions may not be excluded.

Furthermore, it is important to point out that eq 3 is a simple illustration of the concept of capacitive current, but it may not totally describe the hysteresis behavior of PSCs. Indeed, the instant value of the capacitive current is $J = C(V,f)f$, where V is the voltage and f is the measuring frequency. As we have shown in Figure 4b, the capacitance of the PSC is strongly frequency dependent, and it increases rapidly at decreasing frequency, which should be taken into account in detailed modeling and may give rise to a variety of behaviors.

The previous findings suggest a new picture for the dynamic behavior of PSCs, which ultimately exerts the great impact of

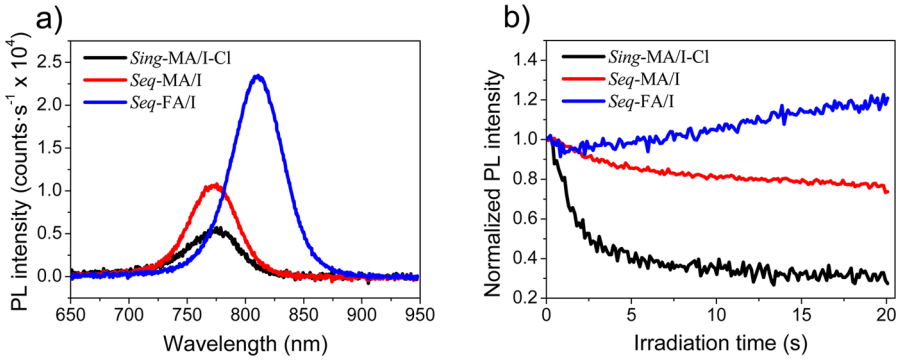

Figure 6. (a) Steady-state PL spectra of the three PS-based devices using a 532 nm laser diode as an excitation source. (b) PL intensity evolution of the PS devices along the irradiation time.

dx.doi.org/10.1021/jz5011187 | *J. Phys. Chem. Lett.* 2014, 5, 2357−2363

the photovoltaic performance. While most solar cells are affected by generation recombination of electronic carriers in a stable structural environment, usually affected also by series transport and charge transfer at interfaces, the ionic and polar framework produces an integral part of the dynamic response of the PSC. Hence, the two aspects shown in Figure 3 reciprocally interact in a nontrivial fashion. It is suggested therefore that slow relaxation constitutes a determinant phenomenon for the rate of electronic processes. As a final demonstration of this contention, we take advantage of the outstanding luminescent properties of the lead halide PS materials. Photoluminescence (PL) is obviously due to the radiative recombination of electrons and holes. While not all recombination need to be radiative, a significant fraction is in the PSCs. Therefore, time evolution of PL provides an additional signature of the coupling of structural relaxation and carrier recombination.

Figure 6a shows the steady-state PL spectra of the three devices studied. Although the absorbances of the samples were relatively comparable (Figure S1, Supporting Information), the intensity of the emission spectra was corrected by the different absorption at the excitation wavelength (λ_{exc} = 532 nm). As can be seen, both MA-based devices showed the emission maxima centered at 772 nm, while the PL of the FA-based PS is centered at 810 nm, which is in agreement with previous results in the literature.[11] Additionally, we registered a sequence of PL spectra throughout the irradiation time under continuous excitation (λ_{exc} = 532 nm), and we observed an unprecedented evolution of the emission intensity over time, Figure 6b. In particular, we observed a strong PL intensity lessening for the sample *Sing*-MA/I-Cl, while the *Seq*-MA/I only experienced a slight decrease. On the contrary, for sample *Seq*-FA/I, the PL intensity was slightly enhanced. Reduction of PL is a reversible process; see Figure S4, Supporting Information. PL is recovered after removal of illumination, keeping the sample in the dark for 20 s. At present, the specific origin of the transient behaviors cannot be unambiguously determined, and more studies will be needed. The PL intensity drop could be associated with an increase of the nonradiative losses upon polarization by increased phonon density due to crystal vibrations, thus reducing the radiative recombination, or simply to an increase of charge separation rate toward regions as grain boundaries where radiative emission is reduced. Additionally, the PL decrease could be ascribed to an abrupt change in the absorption spectrum of the PS upon illumination as a consequence of the dielectric polarization. Last but not least, the PL decrease could arise from an anisotropic absorption of the different light polarization angles upon reaching the dielectric polarization of the device. Because the PL spectra were registered by using an elliptically polarized laser light source (532 nm), the PS samples prepared by the different methodologies could present different crystal orientations and morphologies, which could induce a preferential photon absorption depending on the polarization angle of light. This hypothesis would be compatible with the slight PL enhancement for the *Seq*-FA/I sample. Nevertheless, further studies involving the variation of the linearly polarized angles and the use of circularly polarized light are required to clarify this phenomenon.

In summary, we report the observation of slow dynamic processes in PSCs. The characteristic time of this process has been measured with TPD and IS, obtaining good agreement. The values obtained depend strongly on the PS growth process and on the organic cation, MA or FA. These times are commonly related with the lifetime in other photovoltaic devices, but in PSCs, we have demonstrated that they do not correlate exclusively with recombination processes. An additional slow rearrangement process has been observed for PSCs. We suggest that it could be related to the polarizability of PS, and it is influenced by the PS grain size and the nature of the organic cation. We have observed also a correlation of this slow dynamic process with J/V hysteresis and slow processes detected in PL. Further research is needed to establish the exact mechanisms and how it affects cell performance. However, in any case, a slow dynamic process in PSCs could have enormous implications in the development of PSCs and in the design of novel hybrid PS-based devices.

■ ASSOCIATED CONTENT

Supporting Information

Methods, light absorption, negative capacitance, J/V curves under dark, and photoluminescence reversibility. This material is available free of charge via the Internet at http://pubs.acs.org.

■ AUTHOR INFORMATION

Corresponding Authors

*E-mail: npark@skku.edu (N.-G.P.).
*E-mail: sero@uji.es (I.M.-S.).
*E-mail: bisquert@uji.es (J.B.).

Notes

The authors declare no competing financial interest.

■ ACKNOWLEDGMENTS

This work was supported by MINECO of Spain under Project MAT2013-47192-C3-1-R), Universitat Jaume I Project 12I361.01/1, and National Research Foundation of Korea (NRF) grants funded by the Korea government (MSIP) (No. 2008-0061903) and NRF-2012M3A6A7054861 (Global Frontier R&D Program on Center for Multiscale Energy System).

■ REFERENCES

(1) Park, N.-G. Organometal Perovskite Light Absorbers toward a 20% Efficiency Low-Cost Solid-State Mesoscopic Solar Cell. *J. Phys. Chem. Lett.* **2013**, *4*, 2423−2429.

(2) Snaith, H. J. Perovskites: The Emergence of a New Era for Low-Cost, High-Efficiency Solar Cells. *J. Phys. Chem. Lett.* **2013**, *4*, 3623−3630.

(3) Burschka, J.; Pellet, N.; Moon, S.-J.; Humphry-Baker, R.; Gao, P.; Nazeeruddin, M. K.; Gratzel, M. Sequential Deposition as a Route to High-Performance Perovskite-Sensitized Solar Cells. *Nature* **2013**, *499*, 316−319.

(4) Kim, H.-S.; Lee, C.-R.; Im, J.-H.; Lee, K.-B.; Moehl, T.; Marchioro, A.; Moon, S.-J.; Humphry-Baker, R.; Yum, J.-H.; Moser, J. E.; et al. Lead Iodide Perovskite Sensitized All-Solid-State Submicron Thin Film Mesoscopic Solar Cell with Efficiency Exceeding 9%. *Sci. Rep.* **2012**, *2*, 591.

(5) Kojima, A.; Teshima, K.; Shirai, Y.; Miyasaka, T. Organometal Halide Perovskites as Visible-Light Sensitizers for Photovoltaic Cells. *J. Am. Chem. Soc.* **2009**, *131*, 6050−6051.

(6) Lee, M. M.; Teuscher, J.; Miyasaka, T.; Murakami, T. N.; Snaith, H. J. Efficient Hybrid Solar Cells Based on Meso-Superstructured Organometal Halide Perovskites. *Science* **2012**, *338*, 643−647.

(7) Wang, J. T.-W.; Ball, J. M.; Barea, E. M.; Webber, J.-A.; Hunang, J.; Mora-Sero, I.; Bisquert, J.; Snaith, H. J.; Nicholas, R. J. Low-Temperature Processed Electron Collection Layers of Graphene/TiO_2 Nanocomposites in Thin Film Perovskite Solar Cells. *Nano Lett.* **2014**, *14*, 724−730.

(8) Im, J.-H.; Lee, C.-R.; Lee, J.-W.; Park, S.-W.; Park, N.-G. 6.5% Efficient Perovskite Quantum-Dot-Sensitized Solar Cell. *Nanoscale* **2011**, *3*, 4088−4093.
(9) Ball, J. M.; Lee, M. M.; Hey, A.; Snaith, H. J. Low-Temperature Processed Meso-Superstructured to Thin-Film Perovskite Solar Cells. *Energy Environ. Sci.* **2013**, *6*, 1739−1743.
(10) Suarez, B.; Gonzalez-Pedro, V.; Ripolles, T. S.; Sanchez, R. S.; Otero, L.; Mora-Sero, I. Recombination Study of Combined Halides (Cl, Br, I) Perovskite Solar Cells. *J. Phys. Chem. Lett.* **2014**, *5*, 1628−1635.
(11) Eperon, G. E.; Stranks, S. D.; Menelaou, C.; Johnston, M. B.; Herz, L. M.; Snaith, H. J. Formamidinium Lead Trihalide: A Broadly Tunable Perovskite for Efficient Planar Heterojunction Solar Cells. *Energy Environ. Sci.* **2014**, *7*, 982−988.
(12) Noh, J. H.; Im, S. H.; Heo, J. H.; Mandal, T. N.; Seok, S. I. Chemical Management for Colorful, Efficient, and Stable Inorganic−Organic Hybrid Nanostructured Solar Cells. *Nano Lett.* **2013**, *13*, 1764−1769.
(13) Pellet, N.; Gao, P.; Gregori, G.; Yang, T. Y.; Nazeeruddin, M. K.; Maier, J.; Grätzel, M. Mixed-Organic-Cation Perovskite Photovoltaics for Enhanced Solar-Light Harvesting. *Angew. Chem., Int. Ed.* **2014**, *53*, 3151−3157.
(14) Koh, T. M.; Fu, K.; Fang, Y.; Chen, S.; Sum, T. C.; Mathews, N.; Mhaisalkar, S. G.; Boix, P. P.; Baikie, T. Formamidinium-Containing Metal-Halide: An Alternative Material for Near-IR Absorption Perovskite Solar Cells. *J. Phys. Chem. C* **2013**, DOI: 10.1021/jp411112k.
(15) Noel, N. K.; Stranks, S. D.; Abate, A.; Wehrenfennig, C.; Guarnera, S.; Haghighirad, A.; Sadhanala, A.; Eperon, G. E.; Pathak, S. K.; Johnston, M. B. Lead-Free Organic−Inorganic Tin Halide Perovskites for Photovoltaic Applications. *Energy Environ. Sci.* **2014**, DOI: 10.1039/C4EE01076K.
(16) Ogomi, Y.; Morita, A.; Tsukamoto, S.; Saitho, T.; Fujikawa, N.; Shen, Q.; Toyoda, T.; Yoshino, K.; Pandey, S. S.; Ma, T.; Hayase, S. $CH_3NH_3Sn_xPb_{(1-x)}I_3$ Perovskite Solar Cells Covering up to 1060 nm. *J. Phys. Chem. Lett.* **2014**, *5*, 1004−1011.
(17) Hao, F.; Stoumpos, C. C.; Cao, D. H.; Chang, R. P. H.; Kanatzidis, M. G. Lead-Free Solid-State Organic−Inorganic Halide Perovskite Solar Cells. *Nat. Photonics* **2014**, *8*, 489−494.
(18) Snaith, H. J.; Abate, A.; Ball, J. M.; Eperon, G. E.; Leijtens, T.; Noel, N. K.; Stranks, S. D.; Wang, J. T.-W.; Wojciechowski, K.; Zhang, W. Anomalous Hysteresis in Perovskite Solar Cells. *J. Phys. Chem. Lett.* **2014**, *5*, 1511−1515.
(19) Kim, H.-S.; Mora-Sero, I.; Gonzalez-Pedro, V.; Fabregat-Santiago, F.; Juarez-Perez, E. J.; Park, N.-G.; Bisquert, J. Mechanism of Carrier Accumulation in Perovskite Thin-Absorber Solar Cells. *Nat. Commun.* **2013**, *4*, 2242.
(20) Frost, J. M.; Butler, K. T.; Brivio, F.; Hendon, C. H.; van Schilfgaarde, M.; Walsh, A. Atomistic Origins of High-Performance in Hybrid Halide Perovskite Solar Cells. *Nano Lett.* **2014**, *14*, 2584−2590.
(21) Miyashita, M.; Sunahara, K.; Nishikawa, T.; Uemura, Y.; Koumura, N.; Hara, K.; Mori, A.; Abe, T.; Suzuki, E.; Mori, S. Interfacial Electron-Transfer Kinetics in Metal-Free Organic Dye-Sensitized Solar Cells: Combined Effects of Molecular Structure of Dyes and Electrolytes. *J. Am. Chem. Soc.* **2008**, *130*, 17874−17881.
(22) Bisquert, J.; Fabregat-Santiago, F.; Mora-Seró, I.; Garcia-Belmonte, G.; Giménez, S. Electron Lifetime in Dye-Sensitized Solar Cells: Theory and Interpretation of Measurements. *J. Phys. Chem. C* **2009**, *113*, 17278−17290.
(23) Bi, D.; Yang, L.; Boschloo, G.; Hagfeldt, A.; Johansson, E. M. J. Effect of Different Hole Transport Materials on Recombination in $CH_3NH_3PbI_3$ Perovskite-Sensitized Mesoscopic Solar Cells. *J. Phys. Chem. Lett.* **2013**, *4*, 1532−1536.
(24) Zhao, Y.; Nardes, A. M.; Zhu, K. Solid-State Mesostructured Perovskite $CH_3NH_3PbI_3$ Solar Cells: Charge Transport, Recombination, and Diffusion Length. *J. Phys. Chem. Lett.* **2014**, *5*, 490−494.
(25) Roiati, V.; Colella, S.; Lerario, G.; De Marco, L.; Rizzo, A.; Listorti, A.; Gigli, G. Investigating Charge Dynamics in Halide Perovskite-Sensitized Mesostructured Solar Cells. *Energy Environ. Sci.* **2014**, *7*, 1889−1894.
(26) Lee, J.-W.; Lee, T.-Y.; Yoo, P. J.; Gratzel, M.; Mhaisalkar, S.; Park, N.-G. Rutile TiO_2-Based Perovskite Solar Cells. *J. Mater. Chem. A* **2014**, *2*, 9251−9259.
(27) Gonzalez-Pedro, V.; Juarez-Perez, E. J.; Arsyad, W.-S.; Barea, E. M.; Fabregat-Santiago, F.; Mora-Sero, I.; Bisquert, J. General Working Principles of $CH_3NH_3PbX_3$ Perovskite Solar Cells. *Nano Lett.* **2014**, *14*, 888−893.
(28) Zaban, A.; Greenshtein, M.; Bisquert, J. Determination of the Electron Lifetime in Nanocrystalline Dye Solar Cells by Open-Circuit Voltage Decay Measurements. *ChemPhysChem* **2003**, *4*, 859−864.
(29) Bisquert, J.; Marcus, R. A. Device Modeling of Dye-Sensitized Solar Cells. *Top. Curr. Chem.* **2013**, DOI: 10.1007/128_2013_471.
(30) Ansari-Rad, M.; Anta, J. A.; Bisquert, J. Interpretation of Diffusion and Recombination in Nanostructured and Energy Disordered Materials by Stochastic Quasiequilibrium Simulation. *J. Phys. Chem. C* **2013**, *117*, 16275−16289.
(31) Bisquert, J.; Vikhrenko, V. S. Interpretation of the Time Constants Measured by Kinetic Techniques in Nanostructured Semiconductor Electrodes and Dye-Sensitized Solar Cells. *J. Phys. Chem. B* **2004**, *108*, 2313−2322.
(32) Dualeh, A.; Moehl, T.; Tétreault, N.; Teuscher, J.; Gao, P.; Nazeeruddin, M. K.; Grätzel, M. Impedance Spectroscopic Analysis of Lead-Iodide Perovskite-Sensitized Solid-State Solar Cells. *ACS Nano* **2014**, *8*, 362−373.
(33) Juarez-Perez, E. J.; Wußler, M.; Fabregat-Santiago, F.; Lakus-Wollny, K.; Mankel, E.; Mayer, T.; Jaegermann, W.; Mora-Sero, I. Role of the Selective Contacts in the Performance of Lead Halide Perovskite Solar Cells. *J. Phys. Chem. Lett.* **2014**, *5*, 680−685.
(34) Fabregat-Santiago, F.; Bisquert, J.; Palomares, E.; Otero, L.; Kuang, D.; Zakeeruddin, S. M.; Grätzel, M. Correlation between Photovoltaic Performance and Impedance Spectroscopy of Dye-Sensitized Solar Cells Based on Ionic Liquids. *J. Phys. Chem. C* **2007**, *111*, 6550−6560.
(35) Boix, P. P.; Larramona, G.; Jacob, A.; Delatouche, B.; Mora-Sero, I.; Bisquert, J. Hole Transport and Recombination in All-Solid Sb_2S_3-Sensitized TiO_2 Solar Cells Using CuSCN as Hole Transporter. *J. Phys. Chem. C* **2011**, *116*, 1579−1587.
(36) Christians, J. A.; Fung, R. C. M.; Kamat, P. V. An Inorganic Hole Conductor for Organo-Lead Halide Perovskite Solar Cells. Improved Hole Conductivity with Copper Iodide. *J. Am. Chem. Soc.* **2014**, *136*, 758−764.
(37) Mora-Seró, I.; Bisquert, J.; Fabregat-Santiago, F.; Garcia-Belmonte, G.; Zoppi, G.; Durose, K.; Proskuryakov, Y.; Oja, I.; Belaidi, A.; Dittrich, T.; et al. Implications of the Negative Capacitance Observed at Forward Bias in Nanocomposite and Polycrystalline Solar Cells. *Nano Lett.* **2006**, *6*, 640−650.
(38) Fabregat-Santiago, F.; Mora-Seró, I.; Garcia-Belmonte, G.; Bisquert, J. Cyclic Voltammetry Studies of Nanoporous Semiconductors. Capacitive and Reactive Properties of Nanocrystalline TiO_2 Electrodes in Aqueous Electrolyte. *J. Phys. Chem. B* **2003**, *107*, 758−768.
(39) Yang, X.; Yanagida, M.; Han, L. Reliable Evaluation of Dye-Sensitized Solar Cells. *Energy Environ. Sci.* **2013**, *6*, 54−66.
(40) D'Innocenzo, V.; Grancini, G.; Alcocer, M. J. P.; Kandada, A. R. S.; Stranks, S. D.; Lee, M. M.; Lanzani, G.; Snaith, H. J.; Petrozza, A. Excitons Versus Free Charges in Organo-Lead Tri-Halide perovskites. *Nat. Commun.* **2014**, *5*, 3586.
(41) Ryu, S.; Noh, J. H.; Jeon, N. J.; Kim, Y. C.; Yang, W. S.; Seo, J. W.; Seok, S. I. Voltage Output of Efficient Perovskite Solar Cells with High Open-Circuit Voltage and Fill Factor. *Energy Environ. Sci.* **2014**, DOI: 10.1039/C4EE00762J.